Research article

# Three-field FEM for analysis of thin elastic shells

*Yu.V. Klochkov[1]* (ID) *, A.P. Nikolaev[1]* (ID) *, V.A. Pshenichkina[2]* (ID) *, O.V. Vakhnina[1]* ✉ (ID) *,*

*M.Yu. Klochkov[2]* (ID)

[1] *Volgograd State Agrarian University, Volgograd, Russian Federation*

[2] *Volgograd State Technical University, Volgograd, Russian Federation*

✉ *ovahnina@bk.ru*

**Keywords:** three-field functional, finite element method, strain tensor, curvature tensor, forces, moments

**Abstract.** To obtain a finite element algorithm in the three-field formulation, a conditional functional was used, based on the equality of the actual work of the internal force factors (internal forces and moments) at the strains and curvatures of the middle surface. As an addition, the functional assumed the condition that the work of the residual of internal forces at the strains and curvatures of the middle surface had been equal to zero. The difference between the adopted internal forces and the internal forces represented through the strains and curvatures of the middle surface according to Hooke's law was used as the residual of internal forces. A quadrilateral fragment of the middle surface of a thin shell was used as the finite element. Kinematic quantities (displacements and their first order derivatives), strain quantities (strains and curvatures of the middle surface) and force quantities (internal forces and moments) were taken as the nodal unknowns. Approximating expressions with Hermite polynomials of third degree were used to approximate kinematic quantities. The sought strain and force quantities were approximated through the corresponding nodal unknowns by bilinear shape functions. A finite element stiffness matrix (with the dimensions 36x36) with respect to the kinematic nodal unknowns was formed through the functional minimization. Specific examples showed the efficiency of the three-field finite element algorithm in determining the displacements, strains and internal forces.

## 1. Introduction

*Definition of the object of study.* Taking into account the fairly widespread use of the theoretically based [1, 2] shell systems and objects (domes, roofs, floors, architectural forms, etc.) in various sectors of the construction industry, the development and improvement of methods of numerical analysis of the stress-strain state (SSS) of thin-walled structures made of shells and their fragments is a topical issue.

*Literature review.* Currently, researchers are choosing the finite element method (FEM) in various formulations as the main tool for numerical analysis of the SSS of shell structures. FEM in the formulation of the displacement method has become especially widespread. For example, when determining the SSS of shell and plate structures [3–7], when finding strength indicators of shell structures [8–13], in stability problems [14–16] as well as in composite structures [17] and in thin-walled structures with geometric imperfections [18, 19].

In recent years, for the numerical analysis of the SSS of engineering structures, the FEM in a mixed formulation has come into use for beams and plates analysis [20–23] as well as for shells analysis [24–26].

When comparing the above-mentioned FEM formulations with each other, it should be noted that the mixed FEM formulation has significant advantages, since in this case the conditions of compatibility between the finite elements are satisfied not only for displacements, but also for internal forces and moments. In addition, when solving a finite-element problem applying the mixed formulation, the researcher has an opportunity to simultaneously obtain both kinematic and force parameters of the SSS of the object under study.

*Purpose and objectives of the study.* When performing the numerical analysis of the SSS of thin-walled structures made of shells and their fragments, the finite element algorithm, which allows one to simultaneously study the fields of displacements, strains, internal forces and moments of the shell structure, i.e. a three-field FEM, seems to be the most preferable FEM variant.

In this paper, the above-mentioned three-field FEM is presented in a two-dimensional formulation based on the modified conditional Lagrange functional, and implemented by the example of the finite element analysis of an ellipsoidal elastic shell.

## 2. Materials and methods

In order to obtain a mixed finite element being a fragment of the middle surface of a shell structure, a conditional Lagrange functional is proposed, written in the following form

$$\Phi_L = \frac{1}{2}\int_F \{S_c\}^T \{\varepsilon_c\}\, dF - \frac{1}{2}\int_F \{U\}^T \{q\}\, dF - \frac{1}{2}\int_F \{\varepsilon_c\}^T \left[\{S_c\}-[h]\{\varepsilon_c^k\}\right] dF, \qquad (1)$$

where $\{S_c\}^T_{1\times6} = \left\{N^{11} N^{22} N^{12} M^{11} M^{22} M^{12}\right\}$ is the row of internal forces and moments;

$\{\varepsilon_c\}^T_{1\times6} = \left\{\varepsilon_{11} \varepsilon_{22}\, 2\varepsilon_{12}\, \aleph_{11}\, \aleph_{22}\, 2\aleph_{12}\right\}$ is the row of strains and curvatures at the point $M$; $\{U\}^T_{1\times3} = \{u\ v\ w\}$

are the components of the displacement vector of the point $M$; $\{q\}^T_{1\times3} = \{q_1\ q_2\ q_3\}$ is the row of the

surface load of the shell structure.

In the functional (1), the column $\{\varepsilon_c\}$ is also represented as a matrix expression of the relation with the column $\{S_c\}$ based on Hooke's law [2] and the expression based on Cauchy relations

$$\{S_c\}_{6\times1} = [h]_{6\times6}\{\varepsilon_c\}_{6\times1}; \quad \{\varepsilon_c^k\}_{6\times1} = [D]_{6\times3}\{U\}_{3\times1}, \qquad (2)$$

where $[D]_{6\times3}$ is the matrix of differential operators.

The internal forces and moments as well as the strains and curvatures included into the structure of the columns $\{S_c\}$ and $\{\varepsilon_c\}$ are expressed through their nodal values by the means of the bilinear dependences

$$N^{\alpha\beta} = \{\varphi\}^T_{1\times4} \left\{N^{\alpha\beta i} N^{\alpha\beta j} N^{\alpha\beta k} N^{\alpha\beta l}\right\}; \quad M^{\alpha\beta} = \{\varphi\}^T_{1\times4} \left\{M^{\alpha\beta i} M^{\alpha\beta j} M^{\alpha\beta k} M^{\alpha\beta l}\right\};$$

$$\varepsilon_{\alpha\beta} = \{\varphi\}^T_{1\times4} \left\{\varepsilon_{\alpha\beta}^i\ \varepsilon_{\alpha\beta}^j\ \varepsilon_{\alpha\beta}^k\ \varepsilon_{\alpha\beta}^l\right\}; \quad \aleph_{\alpha\beta} = \{\varphi\}^T_{1\times4} \left\{\aleph_{\alpha\beta}^i\ \aleph_{\alpha\beta}^j\ \aleph_{\alpha\beta}^k\ \aleph_{\alpha\beta}^l\right\}. \qquad (3)$$

The components of the displacement vector of the point $M$ of the middle surface $u,\ v,\ w$ included into the column $\{U\}$ are interpolated in the local coordinate system through their nodal values and their partial first order derivatives by means of the shape functions, with the Hermite polynomials of third degree being the elements of those [25, 26]

$$u = \{\psi\}^T_{1\times12} \{u_y^L\}_{12\times1}; \quad v = \{\psi\}^T_{1\times12} \{v_y^L\}_{12\times1}; \quad w = \{\psi\}^T_{1\times12} \{w_y^L\}_{12\times1}. \qquad (4)$$

Taking into account (3) and (4), it is possible to assemble the following interpolative matrix dependences

$$\{S_c\}_{6\times1} = [H]\{S_y\}_{24\times1}; \quad \{\varepsilon_c\}_{6\times1} = [H]\{E_y\}_{24\times1}; \quad \{U\}_{3\times1} = [A]\{U_y^L\}_{36\times1} = [A][P_R]\{U_y^G\}_{36\times36 \ 36\times1},$$

(5)

where $\{U_y^L\}_{1\times36}^T = \left\{ \{u_y^L\}_{1\times12}^T \ \{v_y^L\}_{1\times12}^T \ \{w_y^L\}_{1\times12}^T \right\}$ is the row of kinematic nodal unknowns in the local coordinate

system; $\{U_y^G\}$ is the column of kinematic nodal unknowns in the global coordinate system; $[P_R]$ is the

matrix dependences between the columns $\{U_y^L\}$ and $\{U_y^G\}$.

Based on the Cauchy relations [1], the column of strains and curvatures $\{\varepsilon_c^k\}$ at the point $M$ included into (1) can be represented in the form of the matrix product

$$\{\varepsilon_c\} = [D]\{U\} = [D][A][P_R]\{U_y^G\} = [B][P_R]\{U_y^G\}.$$

(6)

Taking into account (5), (6), the functional (1) can be transformed into the following form

$$\Phi_L = \frac{1}{2}\{S_y\}^T \int_F [H]^T [h]^{-1} [H] dF \{S_y\} - \frac{1}{2}\{U_y^G\}^T [P_R]^T \int_F [A]\{q\} dF -$$
$$-\frac{1}{2}\{E_y\}^T \int_F [H]^T [H] dF \{S_y\} + \frac{1}{2}\{E_y\}^T \int_F [H]^T [h][B] dF [P_R]\{U_y^G\}.$$

(7)

As a result of the minimization of the functional (7) in $\{S_y\}^T$, $\{E_y\}^T$ and $\{U_y^G\}^T$, the following system of matrix equations can be obtained

$$\begin{cases} \dfrac{\partial \Phi_L}{\partial \{S_y\}^T} = [a]\{S_y\} - [b]^T \{E_y\} = 0; \\[3mm] \dfrac{\partial \Phi_L}{\partial \{E_y\}^T} = -[b]\{S_y\} + [c]\{U_y^G\} = 0; \\[3mm] \dfrac{\partial \Phi_L}{\partial \{U_y^G\}^T} = -\{f_y^G\} + [c]^T \{E_y\} = 0, \end{cases}$$

(8)

where $[a] = \int_F [H]^T [h]^{-1} [H] dF;$ $\quad [b] = \int_F [H]^T [H] dF;$ $\quad \{f_y^G\} = [PR]^T \int_F [A]^T \{q\} dF;$

$[c] = \int_F [H]^T [h][B] dF [PR].$

Based on the second matrix equation of the system (8), the column of the nodal values of the axial forces and bending moments could be expressed

$$\{S_y\} = [b]^{-1}[c]\{U_y^G\}.$$

(9)

Taking into account (9), the first system of equations of the system (8) results in

$$\{E_y\} = \left[[b]^T\right]^{-1}[a][b]^{-1}[c]\{U_y^G\}.$$

(10)

Taking into account (10), the matrix expression for the kinematic nodal unknowns can be determined from the third system of equations of the system (8)

$$[c]^T \left[[b]^T\right]^{-1}[a][b]^{-1}[c]\{U_y^G\} = \{f_y^G\} \tag{11}$$

or in a more compact form

$$\left[K^G\right]\{U_y^G\} = \{f_y^G\}, \tag{12}$$

where $\left[K^G\right] = [c]^T\left[[b]^T\right]^{-1}[a][b]^{-1}[c]$ is the stiffness matrix of a four-node element of discretization.

The stiffness matrix and the column of the nodal internal forces of the shell structure are assembled from the stiffness matrices of four-node elements of discretization $\left[K^G\right]$ and the columns of the nodal internal forces $\{f_y^G\}$ of individual finite elements by means of an index matrix in a standard manner for FEM [9].

The sought kinematic quantities, determined by solving a system of equations for the entire structure using equations (9) and (10), make it possible to determine the nodal values of the axial forces and bending moments $\{S_y\}$ and $\{E_y\}$ for all of the elements, the set of which was used to model the thin-walled shell structure.

The stress fields in the suggested three-field FEM variant can be obtained in two independent ways. The first method is to use the internal force factors obtained through the finite element solution in the formula

$$\sigma^{\alpha\beta} = \frac{N^{\alpha\beta}}{F} + \frac{\xi M^{\alpha\beta}}{I}, \tag{13}$$

where $F$, $I$ are the area and the moment of inertia of the cross section (as applied to a thin-walled shell structure $F = t$; $I = t^3/12$); $\xi$ is the vertical distance from the middle surface point to the cross-section point under consideration.

The second method is to use the calculated strains and curvatures of the matrix $\{E_y\}$ by first passing to the strains at an arbitrary cross-section point located at the distance $\xi \cdot \varepsilon_{\alpha\beta}^{\xi} = \varepsilon_{\alpha\beta} + \xi\aleph_{\alpha\beta}$ from the corresponding point of the middle surface and then using the elasticity matrix $[d]$

$$\{\sigma^{\alpha\beta}\} = [d]\{\varepsilon_{\alpha\beta}^{\xi}\}, \tag{14}$$
$$\underset{3\times1}{\phantom{x}} \quad \underset{3\times3}{\phantom{x}} \quad \underset{3\times1}{\phantom{x}}$$

assembled using of the relations of continuum mechanics [2]

$$\sigma^{\alpha\beta} = \lambda I_1(\varepsilon) g^{\alpha\beta} + 2\mu g^{\alpha\rho} g^{\beta\gamma} \varepsilon_{\rho\gamma}^{\xi}, \tag{15}$$

where $\lambda$, $\mu$ are Lamé parameters; $I_1(\varepsilon) = g^{\alpha\beta}\varepsilon_{\alpha\beta}^{\xi}$, is the first invariant of the strain tensor; $g^{\alpha\beta}$ are the contravariant components of the metric tensor determined at an arbitrary cross-section point of the shell structure.

The correctness and high accuracy of the calculations of the required parameters of the SSS of shell structures applying the developed three-field FEM variant are shown through the examples of solving a number of test problems.

## 3.  Results and Discussion

*Example 1.* A fragment of an elliptical cylinder with a rigidly fixed left generatrix and a free right generatrix loaded with internal pressure with intensity of $q = 0.1$ N/cm² was analyzed (Fig. 1). The

numerical values of the geometric and physical quantities in the example 1 are taken as follows: $b = 0.5$ m; $c = 0.4$ m; $h = 0.01$ m; $L = 0.01$ m; $E = 2 \cdot 10^5$ MPa; the transverse strain coefficient $v = 0.3$.
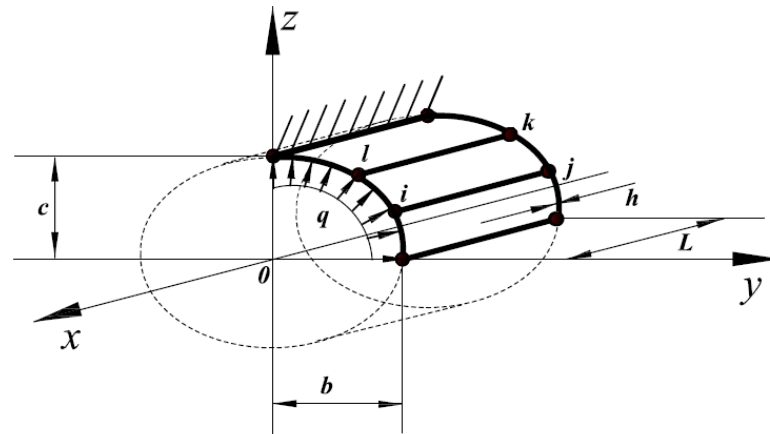


**Figure 1. Analytical scheme of an elliptical cylinder loaded with internal pressure.**

The chosen analytical scheme allows to analytically determine the value of the physical bending moment $M_f^{22}$ at arbitrary point of the elliptical cylinder, having previously resolved the internal pressure into the vertical and horizontal components $q_v$ and $q_g$. Thus, at an arbitrary point $K$ (Fig. 2) the value of the physical bending moment $M_f^{22}$ will be determined by the formula

$$M_f^{22} = q_v z^2 / 2 + q_g (b - y)^2 / 2. \tag{16}$$



**Figure 2. Analytical scheme of the elliptical cylinder section.**

Table 1 gives the values of the "physical" moments $M_f^{22}$ and normal stresses in points $P$, $K$, $T$ of the elliptical cylinder (Fig. 2).

***Table 1. Values of the SSS parameters under control.***

| Discretization mesh |
| --- |

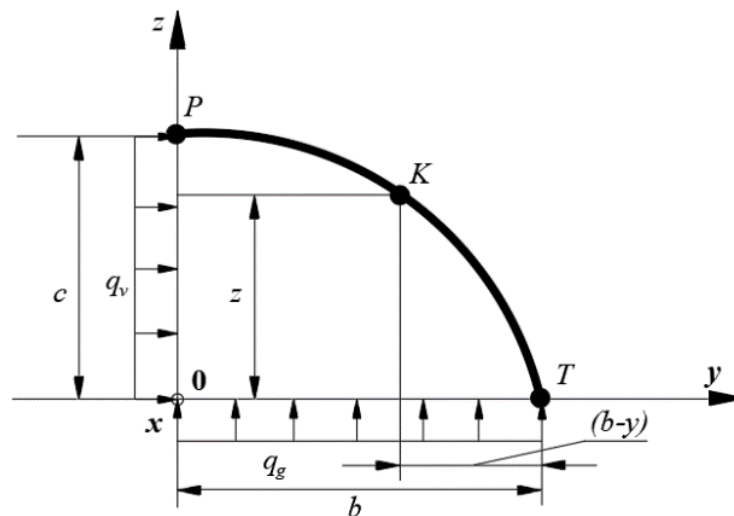| Coordinates of the points, $y;\ t$ | Moments $M_f^{22}$, N·m, stresses $\sigma$, MPa | $31 \times 2$ | $61 \times 2$ | $91 \times 2$ | $121 \times 2$ | Analytical solution $M_f^{22}$, N·m, $\sigma_{tt} = M_f^{22}/W$ |
|---|---|---|---|---|---|---|
| Rigid fixing, $y = 0$, $t = 0$ | $M_f^{22}$ | 2.0495 | 2.0499 | 2.0499 | 2.04997 | 2.050 |
| | $\sigma_{tt}^{in}$ | 12.44 | 12.44 | 12.44 | 12.44 | 12.3 |
| | $\sigma_{tt}^{out}$ | -12.16 | -12.16 | -12.16 | -12.16 | |
| Point $K$, $y = b/\sqrt{2}$, $t = \pi/4$ | $M_f^{22}$ | 0.50705 | 0.5072 | 0.50721 | 0.50722 | 0.50723 |
| | $\sigma_{tt}^{in}$ | 3.084 | 3.09 | 3.09 | 3.09 | 3.043 |
| | $\sigma_{tt}^{out}$ | -2.993 | -3.00 | -3.00 | -3.00 | |
| Point $T$, $y = b$, $t = \pi/2$ | $M_f^{22}$ | 0.00036 | 0.00009 | 0.00004 | 0.00002 | 0.000 |
| | $\sigma_{tt}^{in}$ | 0.00215 | -0.0006 | -0.00025 | -0.00014 | 0.000 |
| | $\sigma_{tt}^{out}$ | 0.0005 | 0.0005 | 0.00024 | 0.00013 | |

The normal stresses values were calculated using the formula (14), i.e. using the previously obtained values of strains and curvatures $\{E_y\}$. The rightmost column shows the values of the bending moment $M_f^{22}$ calculated using the formula (16) and the values of the normal stresses calculated using the formula $\sigma_{tt} = M_f^{22}/W$ ($W$ is the moment of resistance of the cross section). Analysis of the data in Table 1 shows a stable convergence of the calculating process as the discretization mesh becomes finer, and there is an almost complete coincidence of the values of the moments calculated according to the developed algorithm with the values obtained analytically through the formula (16). The calculation error for $M_f^{22}$ is 0.005 %.
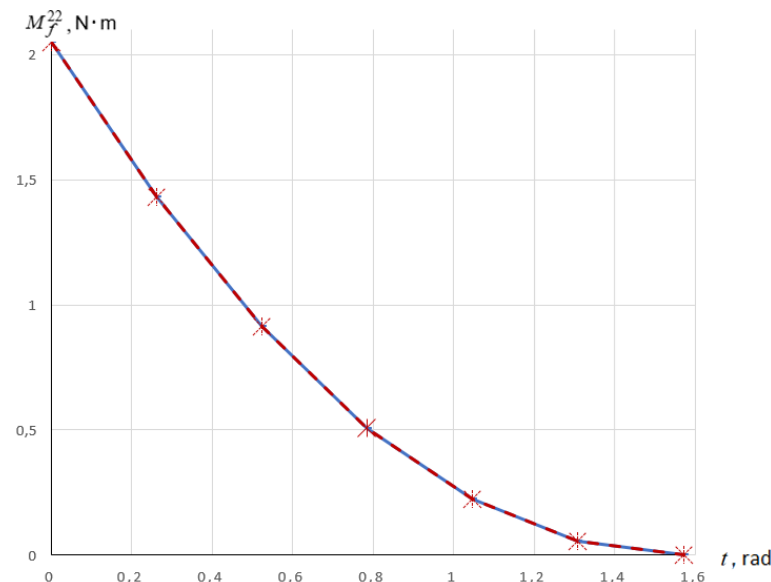


**Figure 3. Curve of the dependence of the bending moment $M_f^{22}$ on the parameter $t$.**

Figure 3 shows the curve of the dependence of the bending moment $M_f^{22}$ on the parameter $t$. The value $t = 0$ corresponds to the rigid fixing (point $P$ in Fig. 2), and the value $t = \pi/2$ corresponds to the

free edge (point $T$ in Fig. 2). The marks in the shape of asterisks on the curve indicate the values of $M_f^{22}$ calculated with the formula (16) based on the static equilibrium condition. The graph shows that the numerical and analytical values of $M_f^{22}$ completely coincide.

*Example 2.* An analysis of the elliptical ring, the analytical scheme of which is shown in Fig. 4, was carried out. Due to the symmetry of the ring, only a quarter of it was used in the analysis. The numerical values of the geometric and physical quantities of the shell were taken as follows: $q = 10$ N/m; $E = 2 \cdot 10^5$ MPa; $\nu = 0.3$; $b = 0.5$ m; $c = 0.2$ m; $h = 0.001$ m; $L = 0.01$ m.
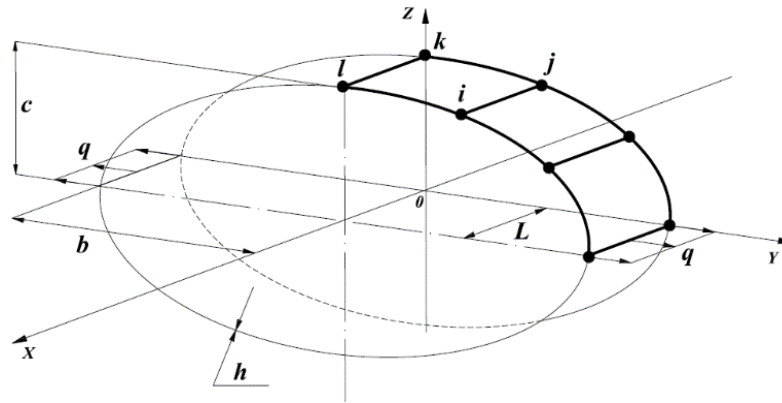


**Figure 4. Analytical scheme of the elliptical ring.**

Table 2 gives the values of the bending moments $M_f^{22}$, the internal forces $N_f^{22}$ and the normal stresses at the points of the analytical scheme (Fig. 4) marked with the coordinates $y$, $t$.

*Table 2. Values of the controlled SSS parameters.*

| Coordinates of the points, $y$; $t$ | Moments $M_f^{22}$, N·m, axial force $N$, N, stresses $\sigma_{xx}$, $\sigma_{tt}$, $10^{-2}$ MPa | Discretization mesh | | | | Values $M_f^{22}$ and $\sigma_{tt}$ calculated with the formulas of the strength of materials [27] |
|---|---|---|---|---|---|---|
| | | $31 \times 2$ | $61 \times 2$ | $91 \times 2$ | $121 \times 2$ | |
| $y = 0$, $t = 0$ | $M_f^{22}$ | -0.55334 | -0.55316 | -0.55312 | -0.55311 | - |
| | $N_f^{22}$ | 0.10437 | 0.10441 | 0.10442 | 0.10442 | 0.100 |
| | $\sigma_{tt}^{in}$ | 333.39 | 333.09 | 333.04 | 333.02 | - |
| | $\sigma_{tt}^{out}$ | -331.13 | -330.83 | -330.77 | -330.75 | - |
| | $\sigma_{xx}^{in}$ | 100.01 | 99.93 | 99.91 | 99.91 | - |
| | $\sigma_{xx}^{out}$ | -99.34 | -99.25 | -99.23 | -99.23 | - |
| $y = b$, $t = \pi/2$ | $M_f^{22}$ | 1.450 | 1.448 | 1.447 | 1.447 | 1.450 |
| | $\sigma_{tt}^{in}$ | -871.61 | -873.03 | -873.30 | -873.40 | 870.0 |
| | $\sigma_{tt}^{out}$ | 860.81 | 862.19 | 862.46 | 862.56 | |
| | $\sigma_{xx}^{in}$ | -261.16 | -261.89 | -261.99 | -262.02 | - |
| | $\sigma_{xx}^{out}$ | 258.54 | 258.68 | 258.74 | 258.77 | - |

The rightmost column of Table 2 gives the values of the bending moment at the points of application of the load, taken from [27]. The normal stresses in the right column are determined through the bending moment using the formula of the strength of materials.

The analysis of the data in Table 2 shows a stable convergence of the calculation process sought parameters and a coincidence in the values of the compared quantities of the bending moments. The calculation error for the bending moment was 0.14 %. Based on the static equilibrium condition $\left( \sum N_x = 0 \right)$ the value of the axial force $N_f^{22}$ at the leftmost point of the analyzed quarter of the ring should be equal to $N_f^{22} = q_v \cdot L = 0.1$ N. The obtained value of the axial force differs from the exact value by 4 %. However, it should be noted here that a larger value of the calculation error in the axial force as compared to the small error in the bending moment is explained by the fact that the axial force value is much smaller than the bending moment value, the contribution of which to the normal stress value is determining.

*Example 3.* A problem of determination of the SSS of a fragment of an elliptical cylinder was solved with the same support conditions as in example 1, which is loaded with a combined external load in the form of internal pressure with intensity of $q = 0.1$ N/cm² and a linearly distributed load with intensity of $q_w = q_v = 1$ N/cm (Fig. 5).
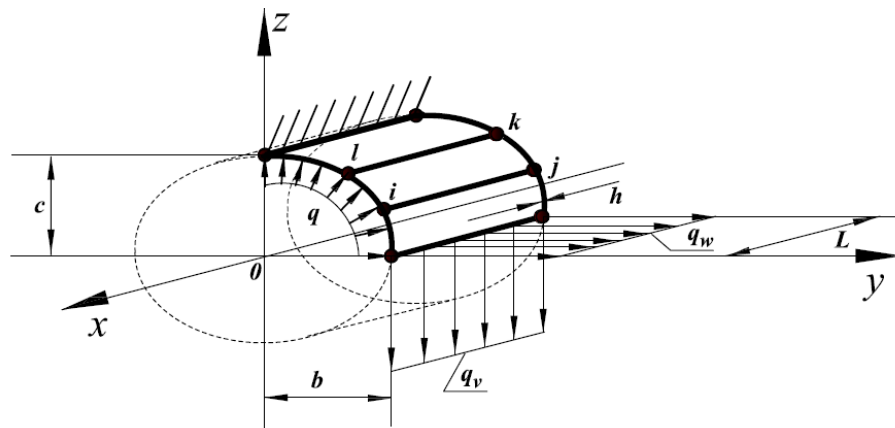


**Figure 5. Analytical scheme of an elliptical cylinder loaded with a combined external load.**

The values of the parameters of the cross-sectional ellipse were taken equal to $b = 0.5$ m; $c = 0.1$ m; with the wall thickness of $h = 0.01$ m; $L = 0.01$ m; $E = 2 \cdot 10^5$ MPa; $\nu = 0.3$.

The analysis of the adopted shell was carried out based on FEM in two formulations:

– based on displacement method formulation [13];

– based on three-field formulation presented in this article.

The results of the analysis are given in Table 3, where the values of the normal stresses $\sigma_{tt}$, $\sigma_{xx}$ and the bending moments at the points of the analytical scheme (Fig. 5) are given depending on the dimension of the discretization mesh. The rightmost column shows the values of $M_f^{22}$, $N_f^{22}$, $\sigma_{tt}$, $\sigma_{xx}$ analytically from the static equilibrium condition, for example, the bending moment in a rigid fixing is determined by the formula

$$M_f^{22} = q\left( c^2/2 + b^2/2 \right) = q_v \cdot L \cdot b + q_w \cdot L \cdot c =$$

$$= 0.1\left( 10^2/2 + 50^2/2 \right) - 1.0 \cdot 1.0 \cdot 50 + 1.0 \cdot 1.0 \cdot 10 = 90.0 \cdot \text{N} \cdot \text{cm}.$$

At the free edge of the shell, the values of the $N_f^{22}$ and normal stress are equal

$$N_f^{22} = q_v \cdot L = 1.0 \cdot 1.0 = 1\,\text{N};$$

$$\sigma_{22}^{midl} = N_f^{22}/F = 1H/1.0 \cdot 1.0\,\text{cm}^2 = 1\,\text{N}/\text{cm}^2,$$

and the value of the $M_f^{22}$ should be equal to zero $\left( M_f^{22} = 0.000 \right)$.

**Table 3. Values of the controlled SSS parameters.**

| Coordinates of the points, $y$; $t$ | Moments $M_f^{22}$, $10^{-2}$ N·m, internal force $N_f^{22}$, N, Stresses $\sigma_{22}$, $10^{-2}$ MPa | Three-field FEM | | | | Displacement method | | | | | Analytical solution $M_f^{22}$, $10^{-2}$ N·m, $N_f^{22}$, N, $\sigma_{11}=\nu\sigma_{22}$, $\sigma_{22}==M_f^{22}/W$, $10^{-2}$ MPa |
|---|---|---|---|---|---|---|---|---|---|---|---|
| | | Mesh of nodes | | | | | | | | | |
| | | 71×2 | 91×2 | 121×2 | 151×2 | 71×2 | 91×2 | 121×2 | 151×2 | 181×2 | |
| Point $P$, $y=0$, $t=0$ | $M_f^{22}$ | 89.87 | 89.90 | 89.93 | 89.94 | 87.89 | 89.18 | 89.70 | 89.85 | 89.91 | 90.0 |
| | $\sigma_{22}^{in}$ | 539.4 | 539.6 | 539.8 | 539.9 | 530.4 | 538.1 | 541.3 | 542.2 | 542.5 | 540.0 |
| | $\sigma_{22}^{out}$ | -539.0 | -539.2 | -539.4 | -539.5 | -524.3 | -532.0 | -535.1 | -536.0 | -536.4 | |
| | $\sigma_{xx}^{in}$ | 162.3 | 162.3 | 162.4 | 162.4 | 159.1 | 161.4 | 162.4 | 162.7 | 162.8 | 162.00 |
| | $\sigma_{xx}^{out}$ | -161.3 | -161.3 | -161.4 | -161.4 | -157.3 | -159.6 | -160.5 | -160.8 | -160.9 | |
| Point $T$, $y=b$, $t=\pi/2$ | $M_f^{22}$ | 0.0022 | 0.0013 | 0.0007 | 0.0004 | 64.69 | 36.0 | 18.34 | 10.96 | 7.25 | 0.000 |
| | $N_f^{22}$ | 1.006 | 1.0034 | 1.0018 | 1.0011 | 157.0 | 84.27 | 40.55 | 23.10 | 14.78 | 1.000 |
| | $\sigma_{22}^{in}$ | 0.57 | 0.57 | 0.57 | 0.57 | -411.0 | -234.2 | -123.5 | -75.78 | -51.07 | - |
| | $\sigma_{22}^{out}$ | 1.55 | 1.56 | 1.56 | 1.56 | 348.9 | 192.2 | 96.38 | 56.85 | 37.30 | - |
| | $\sigma_{22}^{midl}$ | 1.006 | 1.0034 | 1.0018 | 1.0011 | 157.0 | 84.27 | 40.55 | 23.10 | 14.78 | 1.000 |
| | $\sigma_{xx}^{in}$ | 0.810 | 0.378 | 0.228 | 0.192 | -123.3 | -70.27 | -37.06 | -22.73 | -15.32 | - |
| | $\sigma_{xx}^{out}$ | 0.186 | 0.355 | 0.415 | 0.430 | 104.7 | 57.66 | 28.91 | 17.06 | 11.19 | - |
| | $\sigma_{xx}^{midl}$ | 0.498 | 0.367 | 0.322 | 0.311 | 47.1 | 25.28 | 12.16 | 6.93 | 4.43 | 0.300 |

Analysis of the data in Table 3 shows, that when using three-field FEM a rapid convergence of the calculation process in determining the sought quantities is observed, and there is a practical coincidence of the controlled SSS parameters obtained by using the developed algorithm with the results of the analytical solution at a coarse discretization mesh. In the second variant, a slow rate of convergence of the calculation process could be observed even at a significant refinement of the discretization mesh. If the results of the finite element solutions could be considered satisfactory in the section of support, in which the curvature of the middle surface is insignificant, then at the free edge of the shell, at which the curvature increases significantly, the calculation error remains considerable despite a serious refinement of the discretization mesh.

Based on the above-mentioned comparative evaluation of the FEM analyses of the elliptical cylinder with a significant curvature of the middle surface, we can conclude that it is preferable to use the developed three-field FEM variant rather than the most common FEM variant in the displacement method formulation.

*Example 4.* The developed three-field FEM variant (1) ... (15) demonstrates a significantly greater calculation efficiency as compared to the FEM variant in the form of the displacement method [13] and when solving the problems concerning a concentrated load. To confirm this fact, we can consider a problem of determining the SSS of a cylindrical shell loaded with a concentrated force $P=226.8$ N in the middle, which has a hinged support at the diametrically opposite edge, preventing it from vertical movement (Fig. 6).
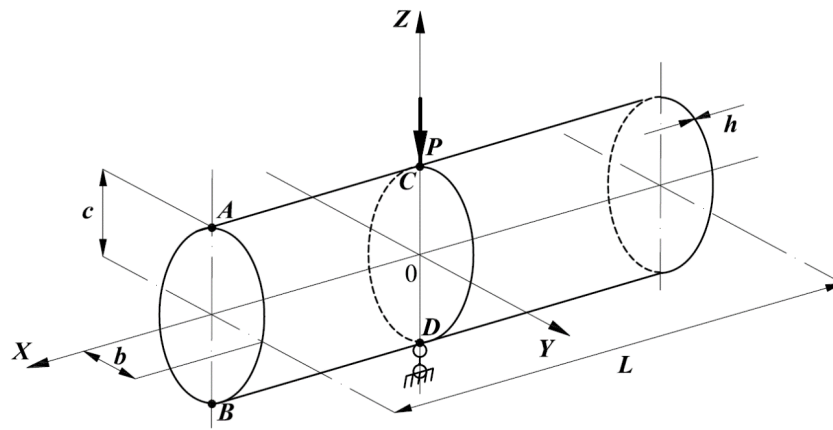
**Figure 6. Analytical scheme of the cylinder loaded with concentrated force $P$.**

Taking into account the symmetry of the analytical scheme, only one quarter of the shell was analyzed. The initial data values were as follows: $L = 26.3$ cm; $h = 0.24$ cm; $E = 7.38 \cdot 10^4$ MPa; $v = 0.3125$. First, a circular cylinder with the radius of $R = 12.6$ cm was analyzed in order to compare the deflection value under the action of the force $P$ with the existing solution presented in [28]. The analysis was performed in two variants: in the first one the three-field FEM variant was used; in the second variant, FEM in the form of the displacement method was used [13]. The results of the analysis are presented in Table 4, which shows the deflection values under the action of the force $P$ and normal stresses $\sigma_{tt}$ at the point $A$ (Fig. 6) at the end of the cylinder during successive refinement of the finite element mesh.

***Table 4. Values of the deflection and normal stresses for the circular cylinder.***

| Deflection $v$, cm; stresses $\sigma_{tt}$, MPa | Variants of the analysis | | | | | | Existing solution [28] |
|---|---|---|---|---|---|---|---|
| | The first variant | | | The second variant | | | |
| | Discretization mesh | | | | | | |
| | $21 \times 21$ | $31 \times 31$ | $41 \times 41$ | $21 \times 21$ | $31 \times 31$ | $41 \times 41$ | |
| $v$ | -0.28781 | -0.28792 | -0.28798 | -0.28748 | -0.28766 | -0.28773 | 0.2889 (Bogner, Fox, Schmitt) |
| $\sigma_{tt}^{in}$ | 21.3224 | 21.0245 | 20.9017 | 22.0884 | 21.7066 | 21.5818 | 0.2865 (Cantin, Klauf) |
| $\sigma_{tt}^{out}$ | -30.5207 | -30.4651 | -30.4669 | -30.5221 | -30.4683 | -30.4869 | 0.2888 (Ashvel, Sabir) |

Analysis of the data in Table 4 shows, that the values of the deflection and stresses turned out to be quite similar in both variants of the analysis. In addition, the deflection values coincide with the existing solutions [28].

However, if an elliptical cylinder replaces the circular one, the calculation results become significantly different. Thus, when the ratio of the semi-axes of the cross-sectional ellipse $b/c$ is equal to four, a large calculation error is observed in the second variant of the analysis. This fact is confirmed by the analysis of the data in Table 5, which gives the values of the deflection under the action of the force $P$ and the values of the stresses $\sigma_{tt}$ at the points $A$ and $B$ (Fig. 6), which should coincide.

*Table 5. Values of the deflection and normal stresses for the elliptical cylinder.*

| Coordinates of the points, $x$; $t$ | Deflection $v$, cm; stresses $\sigma_{tt}$, MPa | Variants of the analysis | | | | | | |
|---|---|---|---|---|---|---|---|---|
| | | The first variant | | | The second variant | | | |
| | | Discretization mesh | | | | | | |
| | | $21\times21$ | $31\times31$ | $41\times41$ | $21\times21$ | $31\times31$ | $41\times41$ | $51\times51$ |
| Point $C(0;0)$ | $v$ | -0.202355 | -0.203385 | -0.203568 | -0.071653 | -0.117069 | -0.163220 | -0.186131 |
| Point $A(26.3;0)$ | $\sigma_{tt}^{in}$ | 17.5780 | 17.3591 | 17.2583 | 11.0566 | 13.4309 | 15.5899 | 16.6424 |
| | $\sigma_{tt}^{out}$ | -20.5413 | -20.4789 | -20.4380 | -12.5950 | -15.5502 | -18.1924 | -19.4827 |
| Point $B(26.3;\pi)$ | $\sigma_{tt}^{in}$ | 17.5541 | 17.3662 | 17.2619 | 1.7814 | 6.9961 | 12.6244 | 15.3878 |
| | $\sigma_{tt}^{out}$ | -20.5711 | -20.4877 | -20.4427 | -2.2496 | -8.3036 | -14.8404 | -18.0619 |

In the first variant of the analysis, it is possible to observe a fast convergence of the calculating process both in terms of the value of the deflection under the action of the force $P$ and in terms of the values of the $\sigma_{tt}$. In addition, the values of the $\sigma_{tt}$ at the points $A$ and $B$ in the first variant turned out to be almost equal to each other even at a coarse (21 × 21) mesh of the discretization elements. In the first variant, the values of the deflection under the action of the force $P$ differ from each other by only 0.6 % at the nodes mesh coarseness of 21 × 21 and 41 × 41. In addition, on the contrary, in the second variant of the analysis, it is possible to observe a rather slow convergence of the calculating process in both the deflection and the stresses as compared to the first variant of the analysis. Thus, the deflection values at the nodes mesh coarseness of 21 × 21 and 51 × 51 differ from each other by a factor of 2.6. The values of $\sigma_{tt}$ at the points $A$ and $B$ significantly differ from each other as well, although they should completely coincide based on the symmetry of the analytical scheme.

The stresses at the points $C$ and $D$ (Fig. 6) should also be equal. Fig. 7 and 8 show the changes in the coefficients $k^{in}$, $k^{out}$ (for each variant), which are the ratios of the stress values at the points $C$ and $D$ of the shell

$$k^{in} = \left(\sigma_{tt}^{in}\right)_C \Big/ \left(\sigma_{tt}^{in}\right)_D \quad \text{and} \quad k^{out} = \left(\sigma_{tt}^{out}\right)_C \Big/ \left(\sigma_{tt}^{out}\right)_D$$

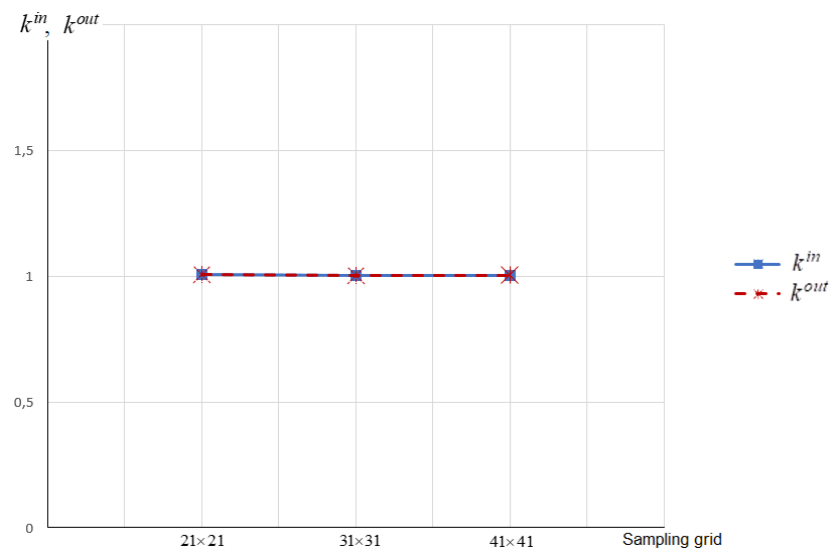depending on the refinement of the discretization mesh.



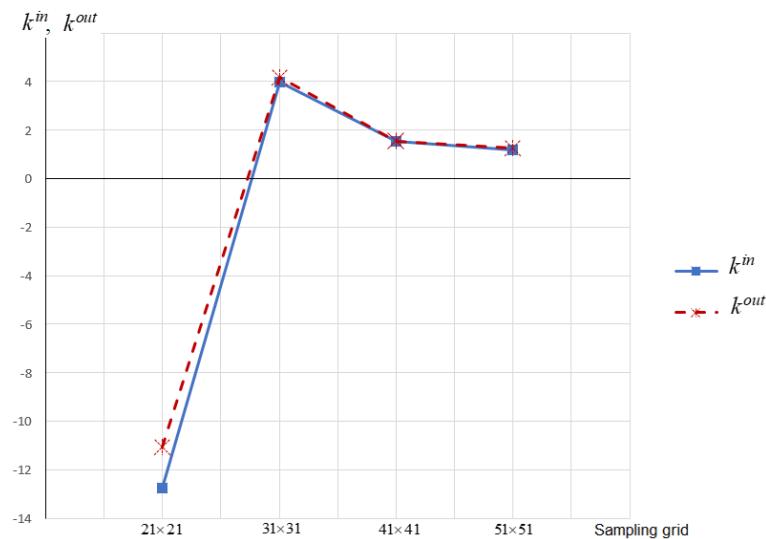**Figure 7. Graphs of the changes in the coefficients $k^{in}$ and $k^{out}$ in the first variant of the analysis.**

**Figure 8. Graphs of the changes in the coefficients $k^{in}$**

**and $k^{out}$ in the second variant of the analysis.**

Fig. 7 shows that, when the developed three-field FEM is used, the values of the coefficients $k^{in}$ and $k^{out}$ are equal to one both at a coarse finite element mesh and in case of its refining, just the way it should be due to the symmetry of the analytical scheme (Fig. 6). When FEM in the form of the displacement method is used, the values of the coefficients $k^{in}$ and $k^{out}$ reach unacceptably large values at a coarse finite element mesh. The coefficients can approach the value of one, if there is a significant refinement of the finite element mesh, which increases the computer time expenditures and enlarges the calculation error being proportional to the total number of the sought unknowns.

Thus, we can conclude that the calculations of the required strength parameters of shells are correct and highly accurate when implementing the developed three-field variant of the FEM.

## 4. Conclusions

Based on the foregoing, the following conclusions can be formulated:

1. The developed three-dimensional FEM variant was implemented using the example of the analysis of a thin-walled shell structure. It allows to simultaneously obtain the fields of displacements, internal force factors and strains of the middle surface of a shell, which significantly expands the capabilities of a detailed numerical analysis of the stress-strain state of such type of structures.

2. The correctness and high accuracy of the calculations of the controlled strength parameters of the SSS of thin-walled shell structures has been proven by solving test problems on the analysis of elliptical cylinders loaded with internal pressure and a linearly distributed load.

3. The calculation error for the values of bending moments was 0.14 %, and it was 4 % for the axial forces values. However, it should be noted here that the normal stress value is mainly determined by the value of the bending moment, while the contribution of the axial force to the value of the stress is minimal.

4. The comparison of two variants of the analyses of an elliptical cylinder with a significant curvature of the middle surface showed substantial advantages of the developed three-field FEM variant. It could be compared to the FEM variant in the displacement method formulation in terms of much higher accuracy of finite element solutions at relatively coarse discretization meshes of the shell.

5. The developed three-field version of FEM has fundamental advantages over the FEM variant in the form of the displacement method, such as indifference to the geometry of the middle surface of the shell and the types of external load.

### References

1. Novozhilov, V.V. Teoriya tonkikh obolochek [Theory of thin shells]. St. Petersburg: St. Petersburg University Publ., 2010. 378 p. (rus)

2. Sedov, L.I. Mekhanika sploshnoy sredy [Mechanics of a continuous medium]. V. 1. Moscow: Nauka, 1976. 536 p. (rus)

3. Lalin, V., Rybakov, V., Sergey, A. The finite elements for design of frame of thin-walled beams. Applied Mechanics and Materials. 2014. 578–579. Pp. 858–863. DOI: 10.4028/www.scientific.net/amm.578-579.858

4. Kirichevsky, R.V., Skrynnykova, A.V. Vliyaniye Approksimiruyushchikh Funktsiy pri Postroyenii Matritsy Zhestkosti Konechnogo Elementa na Skorost' Skhodimosti Metoda Konechnykh Elementov [The effect of approximating functions in the construction of the stiffness matrix of the finite element on the convergence rate of the finite element method]. Tomsk State University Journal of Mathematics and Mechanics. 2019. 57. P. 26. DOI: 10.17223/19988621/57/2 (rus)

5. Tyukalov, Yu.Ya. Quadrilateral Finite Element for Thin and Thick Plates. Construction of Unique Buildings and Structures. 2021. 5 (98). 9802. DOI: 10.4123/CUBS.98.2

6. Agapov, V., Golovanov, R. Comparative analysis of the simplest finite elements of plates in bending. Advances in Intelligent Systems and Computing. 2018. 692. 1009. DOI: 10.1007/978-3-319-70987-1_109

7. Dmitriev, A.N., Lalin, V.V., Novozhilov, Iu.V., Mikhaliuk, D.S. Simulation of Concrete Plate Perforation by Coupled Finite Element and Smooth Particle Hydrodynamics Methods. Construction of Unique Buildings and Structures. 2020. 7 (92). 9207. DOI: 10.18720/CUBS.92.7

8. Rickards, R.B. Metod konechnykh elementov v teorii obolochek i plastin [Finite element method in the theory of shells and plates]. Riga: Zinatne, 1988. 284 p. (rus)

9. Postnov, V.A., Kharkhurim, I.Ya. Metod konechnykh elementov v raschetakh sudovykh konstruktsiy [Finite element method in calculations of ship structures]. Leningrad: Sudostroienie, 1974. 342 p. (rus)

10. Jeon, H.-M., Lee, P.-S., Bathe, K.-J. The MITC3 shell finite element enriched by interpolation covers. Computers & Structures. 2014. 134. Pp. 128–142. DOI: 10.1016/j.compstruc.2013.12.003

11. Ko, Y., Lee P.-S., Bathe, K.-J. A new 4-node MITC element for analysis of two-dimensional solids and its formulation in a shell element. Computers & Structures. 2017. 192. Pp. 34–49. DOI: 10.1016/j.compstruc.2017.07.003

12. Schöllhammer, D., Fries, T.-P. A Higher-order Trace Finite Element Method for Shells. Numerical methods in Engineering. 2021. 122 (5). Pp. 1217–1238. DOI: 10.1002/nme.6558

13. Klochkov, Yu.V., Nikolaev, A.P., Sobolevskaya, T.A., Vakhnina, O.V., Klochkov, M.Yu. The calculation of the ellipsoidal shell based FEM with vector interpolation of displacements when the variable parameterisation of the middle surface. Lobachevskii Journal of Mathematics. 2020. 41 (3). Pp. 373–381. DOI: 10.1134/S1995080220030117

14. Maslennikov, A.M., Kobelev, E.A., Maslennikov, N.A. Solution of sustainability tasks by finite element method. Bulletin of Civil Engineers. 2020. 2 (79). Pp. 68-74. DOI: 10.23968/1999-5571-2020-17-2-68-74

15. Lalin, V.V., Yavarov, A.V., Orlova, E.S., Gulov A.R. Application of the finite element method for the solution of stability problems of the Timoshenko beam with exact shape functions. Power Technology and Engineering. 2019. 4 (53). Pp. 449–454. DOI: 10.1007/s10749-019-01098-6

16. Agapov, V.P., Aidemirov, K.R. Designing of the blades of aircraft propellers by the finite element method, taking into account the strength of structure. RUDN Journal of Engineering Researches. 2021. 1 (22). Pp. 65–71. DOI: 10.22363/2312-8143-2021-22-1-65-71

17. Agapov, V. The Family of Multilayered Finite Elements for the Analysis of Plates and Shells of Variable Thickness. E3S Web of Conferences. 2018 Topical Problems of Architecture. Civil Engineering and Environmental Economics. TPACEE 2018. 2019. Pp. 02013. DOI: 10.1051/e3sconf/20199102013

18. Yakupov, S.N., Kiyamov, H.G., Yakupov, N.M. Modeling a Synthesized Element of Complex Geometry Based Upon Three-Dimensional and Two-Dimensional Finite Elements. Lobachevskii Journal of Mathematics. 2021. 42 (9). Pp. 2263–2271. DOI: 10.1134/S1995080221090316

19. Jiapeng, T., Ping, X., Baoyuan, Z., Bifu, H., A finite element parametric modeling technique of aircraft wing structures. Chinese Journal of Aeronautics. 26 (5). 2013. Pp. 1202–1210. DOI: 10.1016/j.cja.2013.07.019

20. Lalin, V.V., Rybakov, V.A., Ivanov, S.S., Azarov, A.A. Mixed finite-element method in V.I. Slivker's semi-shear thin-walled bar theory. Magazine of Civil Engineering. 2019. 5 (89). Pp. 79–93. DOI: 10.18720/MCE.89.7

21. Tyukalov, Yu.Ya. Finite element model of reisner's plates in stresses. Civil Engineering Journal. 2019. 5 (89). Pp. 61–78. DOI: 10.18720/MCE.89.6

22. Magisano, D., Liang, K., Garcea, G., Leonetti, L., Ruess, M. An efficient mixed variational reduced-order model formulation for nonlinear analyses of elastic shells. International Journal for Numerical Methods in Engineering. 2018. 113 (4). Pp. 634–655. DOI: 10.1002/nme.5629

23. Chernysheva, N.V., Rozin, L.A. Algorithm of Combined Method of 3D Analysis for the Boundary Problems in Infinite Medium. Materials Physics and Mechanics. 2017. 31 (1–2). Pp. 82–85.

24. Gureeva, N.A. Calculation Plainly Loaded Geometrically Nonlinear Designs on the Basis of Mixed FEM with Tenzorno-Vector Approximation Requires Sizes. Izvestiya of Saratov University. MATHEMATICS. MECHANICS. INFORMATICS. 2012. 3 (12). Pp. 56–62. DOI: 10.18500/1816-9791-2012-12-3-56-62. (rus)

25. Klochkov, Yu., Pshenichkina, V., Nikolaev A., Vakhnina, O., Klochkov, M. Stress-strain state of elastic shell based on mixed finite element. Magazine of Civil Engineering. 2023. 4 (120). 12003. DOI: 10.34910/MCE.120.3

26. Klochkov, Yu.V., Pshenichkina, V.A., Nikolaev, A.P., Vakhnina, O.V., Klochkov, M.Yu. Quadrilateral element in mixed FEM for analysis of thin shells of revolution. Structural mechanics of engineering constructions and buildings. 2023. 1 (19). Pp. 64–72. DOI: 10.22363/1815-5235-2023-19-1-64-72

27. Ruditsyn, M.N., Artemov, P.Ya., Lyuboshits, M.I. Spravochnoye posobiye po soprotivleniyu materialov [Reference book on strength of materials]. Minsk: Vysheishaia Shkola Publ., 1970. 630 p. (rus)

28. Sekulovich, M. Metod konechnykh elementov [Finite element method]. Moscow: Stroyizdat, 1993. 664 p. (rus)

**Contacts:**

**Yuri Klochkov,** *Doctor of Technical Sciences*
*ORCID: https://orcid.org/0000-0002-1027-1811*
*E-mail: klotchkov@bk.ru*

**Anatoly Nikolaev**, *Doctor of Technical Sciences*
*ORCID: https://orcid.org/0000-0002-7098-5998*
*E-mail: anpetr40@yandex.ru*


**Valeria Pshenichkina**, *Doctor of Technical Sciences*
*ORCID: https://orcid.org/0000-0001-9148-2815*
*E-mail: vap_hm@list.ru*


**Olga Vakhnina**, *PhD in Technical Sciences*
*ORCID: https://orcid.org/0000-0001-9234-7287*
*E-mail: ovahnina@bk.ru*


**Mikhail Klochkov**,
*ORCID: https://orcid.org/0000-0001-6751-4629*
*E-mail: m.klo4koff@yandex.ru*